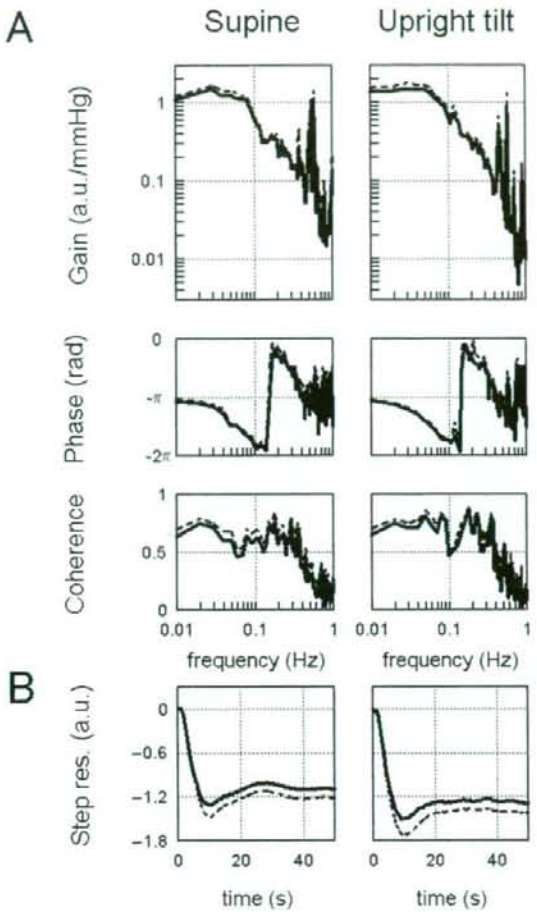

Fig. 5. A: The transfer function of the total baroreflex arc from CSP to AP averaged from all animals (n = 8) in supine (left panels) and 60° upright tilt (right panels) positions. The gain plots (top), phase plots (middle), and coherence function (bottom) are shown. **B**: Step responses (Step res.) derived from the transfer function corresponding to the transfer function shown in A. The transfer function and step response are similar in the supine and upright tilt positions. Solid and dashed lines represent the mean and mean + SD values in A and mean – SD values in B, respectively. a.u., arbitrary unit.

DISCUSSION

Arterial baroreflex is obviously a pivotal mechanism for maintaining AP under orthostatic stress against gravitational fluid shift and pressure disturbance [1, 2, 4], but the baroreflex function and its modulation in upright position are not fully understood. We previously reported that 60° upright tilt resets the steady-state characteristics of the baroreflex neural arc to a higher SNA [5]. However, the dynamic characteristics of the baroreflex system, which is a hallmark of fast-acting neural systems, in upright posture remain to be elucidated. Accordingly, in the present study, we identified the transfer function of the total baroreflex system and its two subsystems. The new major findings are that a 60° upright tilt increases the transfer gain of the baroreflex neural arc (CSP to SNA), decreases the transfer gain of the peripheral arc (SNA to AP), and as a result maintains the dynamic characteristics of the total baroreflex feedback system. These findings support our hypothesis that upright tilt resets dynamic transfer function of baroreflex neural arc to minify the pressure disturbance in total baroreflex control. These results were not affected by the order of postures, since returning the ani-

Table 3. Transfer function of total baroreflex arc (from CSP to AP) in supine, upright tilt and simulated upright tilt positions.

	Supine	Upright tilt	Simulated upright tilt without resetting of the neural arc
Gain (a.u./mmHg)			
0.01 Hz	1.10 ± 0.12	1.38 ± 0.18	0.71 ± 0.18*#
0.1 Hz	0.63 ± 0.09	0.69 ± 0.12	0.41 ± 0.13*#
0.3 Hz	0.15 ± 0.03	0.15 ± 0.03	0.11 ± 0.04*
Phase (rad)			
0.01 Hz	–3.33 ± 0.11	–3.29 ± 0.07	–3.21 ± 0.10
0.1 Hz	–5.76 ± 0.20	–5.55 ± 0.10	–5.51 ± 0.15
0.3 Hz	–1.98 ± 0.25	–1.87 ± 0.23	–1.91 ± 0.24
Coherence			
0.01 Hz	0.63 ± 0.06	0.65 ± 0.05	
0.1 Hz	0.60 ± 0.10	0.61 ± 0.06	
0.3 Hz	0.53 ± 0.07	0.55 ± 0.04	
Step response (mmHg)			
Steady-state level	–1.09 ± 0.11	–1.29 ± 0.12	–0.67 ± 0.11*#

Simulated transfer function in the absence of neural arc resetting is calculated from the neural arc transfer function in supine position and the peripheral arc transfer function in upright tilt position. Values are mean ± SD (n =10). *P < 0.05; supine vs. simulated upright tilt, #P < 0.05; upright tilt vs. simulated upright tilt.

mal posture from 60° upright tilt to horizontal supine position restored the transfer functions to the magnitudes observed in the initial supine position (data not shown).

Little is known about the arterial baroreflex feedback system under orthostatic stress. Although earlier studies investigated the gains of baroreflex control of SNA [12–14], vascular resistance [15] and R-R interval [16], these gains are parts of the total baroreflex system, and thus are insufficient to explain the dynamics of the total arc of the baroreflex feedback system. In addition, no study has examined the phase function of baroreflex in the subsystems and the total system. Moreover, while earlier studies addressed baroreflex in relation to AP regulation under orthostatic stress, most of them evaluated the baroreflex in supine, and not orthostatic posture [14]. In the present study, we identified the transfer functions of the two baroreflex subsystems (the neural and peripheral arcs) in upright posture independently using the baroreflex open-loop technique. Moreover, by connecting the subsystem transfer functions in series and closing them, we revealed the dynamic characteristics of the total baroreflex arc.

Our actual and simulation data indicated that resetting of the baroreflex neural arc in upright posture increases the transfer function gain of the total baroreflex arc. In our experiments, the 60° upright tilt reset and nearly doubled the transfer gain of the neural arc. Although the upright tilt decreased the transfer gain of the peripheral arc, resetting in the neural arc counteracted it and consequently preserved the dynamic transfer gain of the total baroreflex arc (1.4, Table 3). In a simulation of a situation where resetting in the neural arc is absent (Table 3), a 60° upright tilt would decrease the total arc transfer gain. These findings suggest that resetting of the neural arc (that is, baroreflex control of SNA) with dynamic characteristics plays an im-

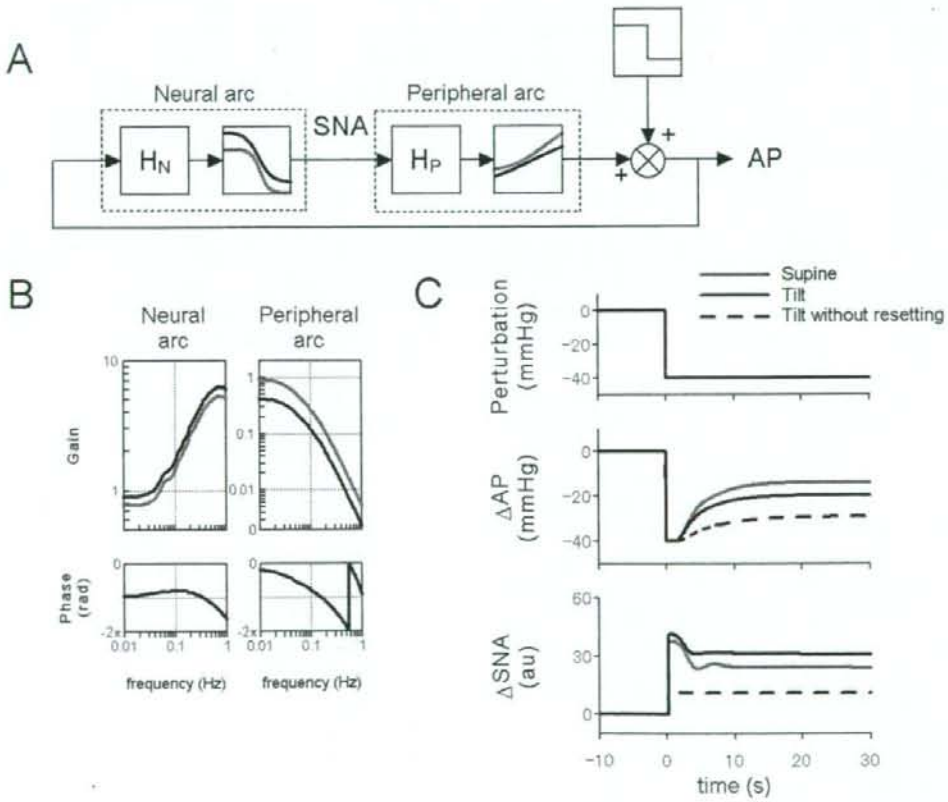

Fig. 6. A: Simulator of the baroreflex system during upright tilt. A stepwise perturbation was applied to the baroreflex negative feedback system (see APPENDIX for details). H_N, neural arc transfer function; H_P, peripheral arc transfer function. Nonlinear sigmoidal functions in the supine and upright tilt positions are shown by gray and black lines, respectively. **B**: Simulation results of integrated dynamic transfer function of linear-sigmoidal nonlinear cascade model in the neural (AP to SNA) and peripheral (SNA to AP) arcs in the supine (gray lines) and upright tilt (black lines) positions. **C**: Simulation results of a closed-loop AP and SNA responses to the stepwise pressure perturbation (–40 mmHg). The resetting during upright tilt (black line) would enhance SNA excitation as compared with the supine position (gray line) to minify a hypotension. Without the resetting in upright tilt, SNA responses would largely be attenuated to lead a hypotension.

portant role to maintain the dynamic transfer function of the total baroreflex system in upright posture.

A simulation of AP stability by baroreflex feedback control against pressure disturbance clearly suggests the importance of resetting of baroreflex neural arc in upright posture. Figure 6 shows the simulation of closed-loop baroreflex control of AP, when pressure disturbance was loaded to the peripheral cardiovascular compartment. According to an earlier study [17], we used the linear-sigmoidal nonlinear cascade model (Fig. 6A) to simulate the baroreflex dynamics. The result of simulation (Fig. 6B) was consistent with our in vivo findings that an upright tilt increased the dynamic transfer gain of the neural arc and decreased the dynamic gain of the peripheral arc. The simulation (Fig. 6C) shows that the baroreflex feedback system would minify the pressure disturbance (40 mmHg) by 50% or more in supine (14 mmHg) and upright tilt (19 mmHg) positions. However, without the resetting of the neural arc in upright tilt, the residual pressure disturbance (29 mmHg) would persist and the velocity of pressure response would become slower (Fig. 6C). These findings suggest that dynamic resetting of the neural arc increases the stability and quickness in response of orthostatic AP against pressure disturbance in closed-loop condition of the total baroreflex arc. In addition, the simulation indicates that the resetting would enhance increases in SNA in response to pressure disturbance in upright tilt compared to supine position (Fig. 6C). Without the resetting in upright tilt, the SNA response would be greatly attenuated (Fig. 6C). This suggests that resetting of the neural arc has a critical role in activating SNA appropriately to prevent hypotension by pressure disturbance during orthostatic stress.

Some explanations for the changes in baroreflex peripheral arc in upright tilt posture may be postulated. First, since the gravitational fluid shift toward the lower part of body (i.e., abdominal vascular bed, lower limbs) during upright posture decreases the preload and effective circulatory blood volume [1, 9], it may attenuate the dynamic transfer function from SNA to AP. Our actual data revealed that upright tilt decreased the transfer gain, but not the transfer phase, of the baroreflex peripheral arc (Fig. 4A). Therefore, upright tilt would blunt the magnitude of AP response to SNA without delaying the response, as shown in the calculated step response (Fig. 4B). Next, increases in humoral factors (i.e., catecholamine, angiotensin II) during upright posture could reduce the dependency of vascular resistance on neural control. However, intravenous infusion of angiotensin II did not affect the transfer function of baroreflex peripheral arc [18]. Moreover, intravenous infusion of catecholamine had no effects on the transfer function from sympathetic stimulation to heart rate [19]. These studies are consistent with the predominance of sympathetic neural control on cardiovascular pressor function [20].

Limitations

The present study has several limitations. First, we excluded the efferent effect of vagally mediated arterial and cardiopulmonary baroreflexes that may affect baroreflex control of SNA. Second, we used an anesthetic agent that may attenuate the baroreflex peripheral arc by reducing the cardiac pumping function, and may affect the neural arc gain. Third, since we sectioned the aortic depressor nerves to open the baroreflex feedback loop, the total baroreflex gain may be lower than the physiological level. Fourth, since we measured only renal SNA, our findings have limited applicability to other SNA. Although static [10, 21] and dynamic [21] regulation of the baroreflex neural arc is similar in renal, cardiac and muscle (vasoconstrictor) SNAs in supine posture, whether this holds true during orthostatic stress remains to be verified.

Lastly, we used rabbits that are quadrupeds. Since humans spend most of their time in nearly 90° upright postures whereas rabbits do not, our findings have limited applicability to humans. However, Japanese White rabbits spend most of their time in 10–40° head-up postures, and frequently stand up to nearly 70°. Since the denervation of both carotid and aortic arterial baroreflexes is known to cause severe postural hypotension at 60° upright tilt in quadrupeds [4], this suggests that even in quadrupeds, arterial baroreflex has a very important function in the maintenance of AP under orthostatic stress. Accordingly, despite the difference in species, our findings may reflect, at least, the qualitative aspects of orthostatic baroreflex physiology in humans. Indeed, recent human studies have suggested that orthostatic stress (lower body negative pressure) enhances the SNA response to AP change [22, 23] and increases baroreflex control of SNA (assessed by the relation between spontaneous changes in diastolic AP and SNA) [12] under baroreflex closed-loop condition.

In conclusion, the transfer function identified in baroreflex open-loop condition showed that 60° upright tilt increases the transfer gain of the baroreflex neural arc, decreases the transfer gain of the peripheral arc, and as a result maintains the dynamic characteristics of the total baroreflex feedback system. Simulation study suggests that resetting of the neural arc increases the transfer gain of the total baroreflex arc and also increases the stability of orthostatic AP against pressure disturbance. These findings suggest that upright tilt resets the dynamic transfer function of the baroreflex neural arc to maintain total baroreflex stability.

APPENDIX

To simulate the closed-loop AP response to stepwise pressure perturbation (Fig. 6), we used the linear-sigmoidal nonlinear cascade model [17].

We modeled the sigmoidal nonlinearity in the baroreflex neural arc by a four-parameter logistic function with

threshold according to our previous study [5] using the following equation:

$$y = \frac{P_1}{1+\exp[P_2(x-P_3)]} + P_4$$

where x and y are input (in mmHg) and output (in au) values. P_1 denotes the response range (in a.u.), P_2 is the coefficient of gain, P_3 is the midpoint of the input range (in mmHg), P_4 is the minimum output value of the symmetric sigmoid curve (in a.u.). We set $P_1 = 94$, $P_2 = 0.10$, $P_3 = 109$, $P_4 = 4$ in the supine position, and $P_1 = 112$, $P_2 = 0.09$, $P_3 = 109$, $P_4 = 29$ during upright tilt, according to our previous study [5].

The sigmoidal nonlinearity in the peripheral arc was modeled by a four-parameter logistic function using the following equation:

$$z = \frac{Q_1}{1+\exp[Q_2(y-Q_3)]} + Q_4$$

where y and z are input (in a.u.) and output (in mmHg) values. Q_1 denotes the response range (in mmHg), Q_2 is the coefficient of gain, Q_3 is the midpoint of the input range (in a.u.), and Q_4 is the minimum output value (in mmHg). We set $Q_1 = 115$, $Q_2 = -0.04$, $Q_3 = 63$, $Q_4 = 50$ in the supine position, and $Q_1 = 82$, $Q_2 = -0.05$, $Q_3 = 88$, $Q_4 = 50$ during upright tilt, according to our previous study [5].

In rabbits, the transfer function of the baroreflex neural arc (baroreceptor pressure to SNA) approximates derivative characteristics in the frequency range below 0.8 Hz, and high-cut characteristics of frequencies above 0.8 Hz [17]. Therefore, according to our previous study [17], we modeled the neural arc transfer function (H_N) using the following equation:

$$H_N(f) = -K_N \frac{1+\frac{f}{f_{c1}}j}{\left(1+\frac{f}{f_{c2}}\right)^2}\exp(-2\pi fjL)$$

where f and j represent the frequency (in Hz) and imaginary units, respectively; K_N is static gain (in a.u./mmHg); f_{c1} and f_{c2} ($fc_1 < f_{c2}$) are corner frequencies (in Hz) for derivative and high-cut characteristics, respectively; and L is a pure delay (in s) that would represent the sum of delays in the synaptic transmission through the baroreflex central pathways and the sympathetic ganglion. The dynamic gain increases in the frequency range of f_{c1} to f_{c2}, and decreases above f_{c2}. In simulations showed in Fig. 6, we matched K_N to the actual data in the supine and upright tilt positions in this study. We also set f_{c1}, f_{c2} and L at 0.05, 0.8 and 0.2, respectively, according to the present and previous studies [17].

In addition, the transfer function of the baroreflex peripheral arc (SNA to AP) approximates a second-order low-pass filter with the dead time as follows:

$$H_P(f) = K_P \frac{1}{1+2\zeta\frac{f}{f_N}j-\left(\frac{f}{f_N}\right)^2}\exp(-2\pi fjL)$$

where f_N and ζ are the neutral frequency (in Hz) and damping ratio, respectively; and L is a pure delay (in s). In simulations showed in Fig. 6, we matched K_P to the actual data in the supine and upright tilt positions in this study. We also set f_N, ζ and L at 0.07, 1.4 and 1.0, respectively, according to the present and previous studies [17].

The input amplitude of the stepwise pressure perturbation was –40 mmHg (Fig. 5, A and C, top panel). The closed-loop AP (Fig. 5C, middle panel) and SNA (Fig. 5C, bottom panel) responses were simulated up to 30 s.

This study was supported by the research project promoted by Ministry of Health, Labour and Welfare in Japan (#H18-nano-ippan-003), the Grants-in-Aid for Scientific Research promoted by Ministry of Education, Culture, Sports, Science and Technology in Japan (#18591992, #20390462) and the Industrial Technology Research Grant Program from New Energy and Industrial Technology Development Organization of Japan.

REFERENCES

1. Rowell LB. Human cardiovascular control. New York: Oxford Univ. Press, 1993.
2. Eckberg DL, Sleight P. Human baroreflexes in Health and Disease. New York: Oxford Univ. Press, 1992.
3. Persson P, Kirchheim H. Baroreceptor reflexes: integrative functions and clinical aspects. Berlin: Springer-Verlag, 1991.
4. Sato T, Kawada T, Sugimachi M, Sunagawa K. Bionic technology revitalizes native baroreflex function in rats with baroreflex failure. Circulation. 2002;106:730-4.
5. Kamiya A, Kawada T, Yamamoto K, Michikami D, Ariumi H, Uemura K, et al. Resetting of the arterial baroreflex increases orthostatic sympathetic activation and prevents postural hypotension in rabbits. J Physiol. 2005;566:237-46.
6. Sato T, Kawada T, Inagaki M, Shishido T, Takaki H, Sugimachi M, et al. New analytic framework for understanding sympathetic baroreflex control of arterial pressure. Am J Physiol. 1999;276:H2251-61.
7. Yamamoto K, Kawada T, Kamiya A, Takaki H, Miyamoto T, Sugimachi M, et al. Muscle mechanoreflex induces the pressor response by resetting the arterial baroreflex neural arc. Am J Physiol. 2004;286:H1382-8.
8. Ikeda Y, Kawada T, Sugimachi M, Kawaguchi O, Shishido T, Sato T, et al. Neural arc of baroreflex optimizes dynamic pressure regulation in achieving both stability and quickness. Am J Physiol. 1996;271:H882-90.
9. Sagawa K, Maughan L, Suga H, Sunagawa K. Cardiac contraction and the pressure-volume relationship. New York: Oxford Univ Press, 1988.
10. Kawada T, Shishido T, Inagaki M, Tatewaki T, Zheng C, Yanagiya Y, et al. Differential dynamic baroreflex regulation of cardiac and renal sympathetic nerve activities. Am J Physiol Heart Circ Physiol. 2001;280:H1581-90.
11. Glantz SA. Primer of Biostatistics (4th ed). New York: McGraw-Hill, 1997.
12. Ichinose M, Saito M, Fujii N, Kondo N, Nishiyasu T. Modulation of the control of muscle sympathetic nerve activity during severe orthostatic stress. J Physiol. 2006;576:947-58.
13. Fu Q, Shook RP, Okazaki K, Hastings JL, Shibata S, Conner CL, et al. Vasomotor sympathetic neural control is maintained during sustained upright posture in humans. J Physiol (Lond). 2006;577:679-87.
14. Mosqueda-Garcia R, Furlan R, Fernandez-Violante R, Desai T, Snell M, Jarai Z, et al. Sympathetic and baroreceptor reflex function in neurally mediated syncope evoked by tilt. J Clin Invest. 1997;99:2736-44.
15. Cooper VL, Hainsworth R. Carotid baroreceptor reflexes in humans during orthostatic stress. Exp Physiol. 2001;86:677-81.
16. Cooke WH, Hoag JB, Crossman AA, Kuusela TA, Tahvanainen KU, Eckberg DL.

Human responses to upright tilt: a window on central autonomic integration. J Physiol. 1999;517:617-28.
17. Kawada T, Yanagiya Y, Uemura K, Miyamoto T, Zheng C, Li M, et al. Input-size dependence of the baroreflex neural arc transfer characteristics. Am J Physiol Heart Circ Physiol. 2003;284:H404-15.
18. Kashihara K, Takahashi Y, Chatani K, Kawada T, Zheng C, Li M, et al. Intravenous angiotensin II does not affect dynamic baroreflex characteristics of the neural or peripheral arc. Jpn J Physiol. 2003;53:135-43.
19. Kawada T, Miyamoto T, Miyoshi Y, Yamaguchi S, Tanabe Y, Kamiya A, et al. Sympathetic neural regulation of heart rate is robust against high plasma catecholamines. J Physiol Sci. 2006;56:235-45.
20. Minson J, Chalmers J, Kapoor V, Cain M, Caon A. Relative importance of sympathetic nerves and of circulating adrenaline and vasopressin in mediating hypertension after lesions of the caudal ventrolateral medulla in the rat. J Hypertens. 1986;4:273-81.
21. Kamiya A, Kawada T, Yamamoto K, Michikami D, Ariumi H, Miyamoto T, et al. Muscle sympathetic nerve activity averaged over 1 minute parallels renal and cardiac sympathetic nerve activity in response to a forced baroreceptor pressure change. Circulation. 2005;112:384-6.
22. Ichinose M, Saito M, Ogawa T, Hayashi K, Kondo N, Nishiyasu T. Modulation of control of muscle sympathetic nerve activity during orthostatic stress in humans. Am J Physiol Heart Circ Physiol. 2004;287:H2147-53.
23. Ichinose M, Saito M, Kitano A, Hayashi K, Kondo N, Nishiyasu T. Modulation of arterial baroreflex dynamic response during mild orthostatic stress in humans. J Physiol. 2004;557:321-30.

Servo-Controlled Hind-Limb Electrical Stimulation for Short-Term Arterial Pressure Control

Authors: Toru Kawada[1], MD, PhD; Shuji Shimizu[1], MD; Hiromi Yamamoto[2], MD; Toshiaki Shishido[1], MD, PhD; Atsunori Kamiya[1], MD, PhD; Tadayoshi Miyamoto[3], PhD; Kenji Sunagawa[4], MD, PhD; Masaru Sugimachi[1], MD, PhD

Affiliation: [1]Department of Cardiovascular Dynamics, Advanced Medical Engineering Center, National Cardiovascular Center Research Institute, Osaka 565-8565, Japan, [2]Division of Cardiology, Department of Internal Medicine, Kinki University School of Medicine, Osaka 589-8511, Japan, [3]Department of Physical Therapy, Faculty of Health Sciences, Morinomiya University of Medical Sciences, Osaka 559-8611, Japan, [4]Department of Cardiovascular Medicine, Graduate School of Medical Sciences, Kyushu University, Fukuoka 812-8582, Japan

Short title: Arterial Pressure Control by Hind-Limb Stimulation

Grants: Supported by "Health and Labour Sciences Research Grant for Research on Advanced Medical Technology", "Health and Labour Sciences Research Grant for Research on Medical Devices for Analyzing, Supporting and Substituting the Function of Human Body", "Health and Labour Sciences Research Grant (H18-Iryo-Ippan-023) (H18-Nano-Ippan-003) (H19-Nano-Ippan-009)", from the Ministry of Health, Labour and Welfare of Japan, "Industrial Technology Research Grant Program" from New Energy and Industrial Technology Development Organization of Japan.

Correspondence: Toru Kawada, MD, PhD
Department of Cardiovascular Dynamics, Advanced Medical Engineering Center, National Cardiovascular Center Research Institute. 5-7-1 Fujishirodai, Suita, Osaka 565-8565, Japan
Phone +81-6-6833-5012 ext. 2427. FAX +81-6-6872-7485
e-mail torukawa@res.ncvc.go.jp

Abstract

Background: Autonomic neural intervention is a promising tool for modulating circulatory system thereby treating some cardiovascular diseases. **Methods and Results:** We examined whether we could control arterial pressure (AP) by acupuncture-like hind-limb electrical stimulation (HES) in eight pentobarbital-anesthetized cats. With a 0.5-ms pulse width, HES monotonically reduced AP as the stimulus current increased from 1 to 5 mA, suggesting that the stimulus current could be a primary control variable. On the other hand, the depressor effect of HES showed a nadir around 10 Hz in the frequency range between 1 and 100 Hz. Dynamic characteristics of the AP response to HES approximated a second-order low-pass filter with dead time (gain: -10.2±1.6 mmHg/mA, natural frequency: 0.040±0.004 Hz, damping ratio 1.80±0.24, dead time: 1.38±0.13 s, mean±SE). Based on these dynamic characteristics we developed a servo-controlled HES system. When a target AP value set at 20 mmHg below the baseline AP, time required for the AP response to reach 90% of the target level was 38±10 s. The steady-state error between the measured and target AP values was 1.3±0.1 mmHg. **Conclusions:** Autonomic neural intervention by acupuncture-like HES may provide an additional modality to quantitatively control the circulatory system.

Keywords: transfer function; proportional-integral controller; systems analysis

Because abnormality in the autonomic nervous system is often associated with cardiovascular diseases, treating cardiovascular diseases by autonomic neural interventions have attracted many researchers.[1-6] Recently, autonomic neural interventions using electronic devices have again the focus of attention as a potential modality for treating cardiovascular diseases resistant to conventional therapeutics. To name a few, chronic vagal nerve stimulation dramatically improves the survival of chronic heart failure after myocardial infarction in rats.[7] Chronic baroreceptor activation enhances the survival of pacing-induced heart failure in dogs.[8] A recent version of device-based treatment of hypertension in human is reported.[9] A framework of electrical neural intervention is also effective to elevate arterial pressure (AP) against hypotensive events.[10-13]

Aside from direct neural stimulation, electroacupuncture can modify autonomic balance thereby treating cardiovascular diseases.[14-16] Although one feature of the electroacupuncture may be its long-lasting effects, immediate cardiovascular responses to acupuncture-like stimulation are also observed in several experimental settings. For example, a sixty-second manual acupuncture-like stimulation of a hind limb reduces renal or cardiac sympathetic nerve activity, causing hypotension and bradycardia in anesthetized rats.[17,18] We have shown that electrical stimulation of a hind limb using acupuncture needles immediately resets the arterial baroreflex and reduces sympathetic nerve activity in anesthetized rabbits.[19] Acupuncture-like hind-limb electrical stimulation (HES) induces immediate hypotension with changes in the relationship between cardiac and renal sympathetic nerve activities in anesthetized cats.[20]

In the present study, we hypothesized that AP could be controlled by HES. Quantification of the dynamic input-output relationship between a given stimulus and the AP response is essential for artificially controlling AP.[10-12] Accordingly the first aim was to identify the dynamic input-output relationship between HES and the AP response. The second aim was to develop a feedback controller system that could reduce AP at a prescribed target level using HES.

Materials and Methods

Surgical Preparation

Animal care was provided in strict accordance with the *Guiding Principles for the Care and Use of Animals in the Field of Physiological Sciences* approved by the Physiological Society of Japan. All protocols were approved by the Animal Subject Committee of National Cardiovascular Center. Eight adult cats weighing from 2.3 to 4.3 kg were anesthetized by an intraperitoneal injection of pentobarbital sodium (30-35 mg/kg) and ventilated mechanically via a tracheal tube with oxygen-supplied room air. The depth of anesthesia was maintained with a continuous intravenous infusion of pentobarbital sodium (1-2 $mg \cdot kg^{-1} \cdot h^{-1}$) through a catheter inserted into the right femoral vein. Vecuronium bromide (0.5-1.0 $mg \cdot kg^{-1} \cdot h^{-1}$, i.v.) was given continuously to suppress muscular activity. AP was measured using a catheter-tip manometer inserted from the right femoral artery and advanced into the thoracic aorta.

Hind-Limb Electrical Stimulation

In the supine position, both hind-limbs were lifted to obtain a better view of the lateral sides of the lower legs. An acupuncture needle with a diameter of 0.2 mm (CE0123, Seirin-Kasei, Japan) was inserted into a point below the knee joint just lateral to the tibia.[20] A 23-gauge needle was inserted into the skin behind the ankle as the ground. HES was applied bilaterally via two independent isolators connected to an electrical stimulator (SEN 7203, Nihon Kohden, Japan) as shown in Figure 1. The pulse width was changed manually whereas the stimulus frequency and the stimulus current were controlled by a dedicated laboratory computer system. The electrical stimulation was started after the hemodynamic effects of needle insertion had disappeared, and the acupuncture needle remained inserted during each protocol.

Protocols

Protocol 1 (n=8). To quantify the AP response to HES as a function of stimulus current and pulse width, we fixed the stimulus frequency at 10 Hz and changed the stimulus current stepwise from 0 to 5 mA in 1-mA increments every minute. The 6-min current test was repeated with an intervening interval of 3 to 5 min using different pulse widths (0.1, 0.2, 0.5 and 1 ms). The order of the pulse-width settings was randomized across the animals.

Protocol 2 (n=8). To quantify the AP response to HES as a function of stimulus frequency and pulse width, we fixed the stimulus current at 3 mA and changed the stimulus frequency sequentially from 0 to 100 Hz (0, 1, 2, 5, 10, 15, 20, 50 and 100 Hz). Each stimulus frequency was maintained for 1 min. The 9-min frequency test was repeated with an intervening interval of 3 to 5 min using different pulse widths (0.1, 0.2, 0.5 and 1 ms). The order of the pulse-width settings was randomized across the animals.

Protocol 3 (n=8). To identify the dynamic input-output relationship between HES and the AP response, we randomly turned HES on and off every 2 s according to a binary white noise sequence for 30 min. The HES setting (0.5-ms pulse width, 10 Hz, 3 mA) was chosen to induce effective hypotension based on the preliminary results obtained from Protocols 1 and 2.

Protocol 4 (n=8). Based on the result of Protocol 3, we designed a feedback controller that could automatically adjust the stimulus frequency and the stimulus current for HES. The pulse width was fixed at 0.5 ms. To examine the performance of the feedback controller, we set a target AP value at 20 mmHg below the baseline AP and activated the feedback controller for 10 min.

The following two supplemental protocols were performed in 3 of the 8 cats. a) We inserted two acupuncture needles into the triceps surae muscle with a distance of approximately 2.5 cm, and examined if changes in AP was associated with direct muscle stimulation (0.5-ms pulse width, 10 Hz, 3 mA). Both hind limbs were stimulated simultaneously using two independent isolators. b) We exposed the sciatic nerve after finishing Protocols 1 through 4, and examined if sectioning the sciatic nerve abolished the hemodynamic effects of HES. Unilateral HES was performed (0.5-ms pulse width, 10 Hz, 3 mA) before and after sectioning the ipsilateral sciatic nerve.

Data analysis

In Protocols 1 and 2, the AP value was obtained by averaging the last 10-s data at each stimulus condition. In Protocol 1, the effect of stimulus current was assessed by changes in AP from the 0-mA stimulus condition for each pulse width. In Protocol 2, the effect of stimulus frequency was assessed by changes in AP from the 0-Hz stimulus condition for each pulse width.

In Protocol 3, the transfer function from HES to AP was estimated by means of an analysis for one-input, one-output systems. Data were first resampled at 10 Hz and segmented into 8 sets of 50%-overlapping bins of 4096 points each. For each segment, a linear trend was subtracted and a Hanning window was applied. Frequency spectra of the input and output were obtained via fast Fourier transformation. Next, the ensemble averages of input power spectral density [$S_{XX}(f)$], output power spectral density [$S_{YY}(f)$], and cross spectral density between the input and output [$S_{YX}(f)$] were calculated over the 8 segments. Finally, the transfer function from input to output [$H(f)$] was calculated as[21]

$$H(f) = \frac{S_{YX}(f)}{S_{XX}(f)} \quad (1)$$

To quantify the linear dependence between the input and output signals in the frequency domain, a magnitude squared coherence function [$Coh(f)$] was also calculated as[21]

$$Coh(f) = \frac{|S_{YX}(f)|^2}{S_{XX}(f)S_{YY}(f)} \quad (2)$$

In Protocol 4, the performance of the feedback controller was evaluated by the time required for the AP response to reach 90% of the target AP decrease and by the standard deviation of the steady-state error between the target and measured AP values during the last 5 min of the 10-min feedback control. These two values were calculated based on the 2-s moving averaged data of AP.

Statistical analysis

All data are presented as means and SE values. In Protocol 1, changes in AP were examined by two-way repeated-measures analysis of variance (ANOVA) using the stimulus current as one factor and the pulse width as the other factor.[22] In Protocol 2, changes in AP were examined by two-way repeated-measures ANOVA using the stimulus frequency as one factor and the pulse width as the other factor. Differences were considered significant when $P<0.05$.

Results

Relationship Between Stimulus Intensity and AP Response

Typical time series of Protocols 1 and 2 obtained from one animal are shown in Figures 2A and 2B, respectively. The pulse width was set in a random order. In Protocol 1, baseline AP obtained at the 0-mA stimulus condition was 118.4±5.4 mmHg across the animals. Changes in mean AP as a function of stimulus current are summarized in Figure 2C. The decrease in AP became greater as the stimulus current increased. The overall statistical analysis indicated that the effect of the stimulus current on the magnitude of AP decrease was significant whereas that of pulse width was not. There was no significant interaction effect between the stimulus current and the pulse width.

In Protocol 2, baseline AP at the 0-Hz stimulus condition was 117.6±5.9 mmHg across the animals. Changes in mean AP as a function of stimulus frequency are summarized in Figure 2D. The decrease in AP became greater as the stimulus frequency increased from 1 to 10 Hz but it became smaller when the stimulus frequency exceeded 10 Hz. At the pulse width of 1 ms, the stimulus frequency of 100 Hz even increased AP. The overall statistical analysis indicated that the effect of stimulus frequency on the magnitude of AP decrease was significant whereas that of pulse width was not. There was no significant interaction effect between the stimulus frequency and the pulse width.

Dynamic Characteristics of AP Response to HES

Figure 3A depicts typical time series obtained from Protocol 3. HES was turned on and off randomly, which decreased the mean level of AP and also caused intermittent AP variations. When HES was finally turned off at 30 min, AP began to increase toward the prestimulation value. A long-lasting effect of HES was not observed in the present protocol. The white line in the AP trace represents the 2-s moving averaged data of AP.

The results of transfer function analysis are depicted in Figure 3B. In the gain plot, the magnitude of AP response relative to the HES input was plotted in the frequency domain. The gain value became smaller as the frequency increased, indicating the low-pass characteristics of the AP response to HES. In the phase plot, AP showed an out-of-phase relationship with HES at the lowest frequency (0.0024 Hz). The phase delayed more with increasing the frequency of modulation. The coherence value was approximately 0.7 in the frequency range below 0.06 Hz. The coherence value became smaller in the frequency range above 0.1 Hz but still retained a value of 0.5, indicating that approximately half of the AP variation was explained by the HES input.

The general feature of the dynamic characteristics of the AP response to HES approximated what is known as a second order low-pass filter with a pure dead time, which is mathematically described as

$$H(f) = \frac{-K}{1 + 2\zeta \frac{f}{f_N} j + \left(\frac{f}{f_N} j\right)^2} \exp(-2\pi f j L) \qquad (3)$$

where K is the steady-state gain, f_N is the natural frequency, ζ is the damping ratio, and L is the pure dead time. When we performed an iterative nonlinear least square fitting using a downhill Simplex method, K, f_N, ζ and L were estimated as 10.2±1.6 mmHg/mA, 0.040±0.004 Hz, 1.80±0.24 and 1.38±0.13 s, respectively. A model transfer function shown in Figure 3C was drawn using K, f_N, ζ and L of 10 mmHg/mA, 0.04 Hz, 2 and 1 s, respectively.

Development of Feedback Controller

We used a classical feedback controller to adjust the stimulus intensity of HES.[23-25] In reference to Figure 4A, a HES command is determined based on a difference between measured and target AP values. $G(f)$ represents the transfer function of the controller with a proportional gain (K_P) and an integral gain (K_I). $H(f)$ indicates the model transfer function shown in Figure 3C. A detailed mathematical description of the controller is supplied in *Appendix A*.

To circumvent a threshold phenomenon in the stimulus current-AP response relationship (see *Appendix B* for details), the HES command (in an arbitrary unit) was transformed into the stimulus current (in mA) by a factor of 1 (Fig. 4B, left) only when the HES command exceeded unity. When the HES command was less than unity, the stimulus current was held at 1 mA and the HES command was transformed into the stimulus frequency (in Hz) by a factor of 10 (Fig. 4B, right). The stimulation was turned off when the HES command became negative.

Several sets of simulations were conducted using the model transfer function. The target AP was set at 20 mmHg below the baseline AP. To mimic the pulse pressure in AP, a 3-Hz sinusoidal wave (corresponding to the HR of 180 beats/min) with an amplitude of 15 mmHg (corresponding to the pulse pressure of 30 mmHg) was added to the AP signal. To avoid pulsatile variation in the HES command, we set the proportional gain at zero. Under this condition, when the integral gain was set at 0.001, AP decreased gradually and it took more than 3 min to reach the target AP (Fig. 4C, left). When the integral gain was set at 0.005, AP decreased more promptly and reached the target AP in less than one minute (Fig. 4C, center). When the integral gain was set at 0.01, the AP response occurred more rapidly but showed significant oscillations before settling (Fig. 4C, right). Based on these simulation results, we set the proportional gain at zero and the integral gain at 0.005 for the actual feedback-control experiment in Protocol 4.

Performance of feedback controller

Figure 5A demonstrates the AP regulation by HES obtained from 2 typical animals. The proportional and integral gains of the controller were not altered among the animals (i.e., $K_P = 0$, $K_I = 0.005$). The white line in the AP trace indicates 2-s moving averaged data. The target AP was set at 20 mmHg below the AP value just before the application of HES. The feedback controller was activated for 10 min, which decreased AP at the target level. The HES command was individualized via the feedback mechanism. In the left panel of Figure 5A, the HES command gradually increased throughout the 10-min regulation. In the right panel of Figure 5A, the HES command was less than unity from 1 to 7 min of the 10-min regulation. In this time period, the HES command altered the stimulus frequency rather than the stimulus current.

Mean and mean±SE values of the HES command averaged from 8 animals are shown in the top panel of Figure 5B. There was a large variance in the HES command among the animals, suggesting inter-individual differences in the responsiveness to HES. The target AP was 102.5±5.6 mmHg across the animals. The error signal between the target AP and measured AP disappeared in less than one minute (Figure 5B, bottom). The time required for the AP response to reach 90% of the target AP decrease was 38±10 s. Thereafter, the error remained very small

until the end of the 10-min regulation. The standard deviation of the steady-state error was 1.3±0.1 mmHg. After the end of the feedback regulation, the error signal gradually returned to approximately 20 mmHg.

Figure 6 represents typical results of the supplemental protocols. Electrical stimulation of the triceps surae muscle (denoted as "MS") did not change AP significantly in spite of visible twitching of the stimulated muscle, suggesting that the depressor response to HES was not the outcome of the direct muscle stimulation (Fig. 6A). Sectioning the ipsilateral sciatic nerve abolished the depressor effect of HES, suggesting that somatic afferent signals were delivered through the sciatic nerve to the central nervous system during HES (Fig. 6B).

Discussion

We identified the dynamic input-output relationship between HES and the AP response. By using the model transfer function from HES to AP, we were able to develop a servo-controller that automatically adjusted the HES command to reduce AP at a prescribed target level.

Development of Feedback Controller

The stimulus current-AP response relationship showed a monotonous decreasing slope (Fig. 2C). Because the effect of the pulse width was statistically insignificant, we chose the stimulus current as a primary control variable. The problem with using the stimulus current for the control variable was that a certain threshold current existed between 0 and 1 mA where the AP response to EA became discontinuous. If the stimulus current happened to be feedback controlled near the threshold current, AP showed significant oscillation around the target level (Fig. 7, see *Appendix B* for details). To avoid such a problem related to the threshold current, we set the minimum current to 1 mA (above the threshold current) and employed the stimulus frequency as a secondary control variable (Fig. 4B).

The stimulus frequency-AP response relationship revealed a valley-shaped curve with the nadir around 10 Hz (Fig. 2D). The result is similar to that obtained by stimulating hamstring muscle afferent nerves.[26] From the viewpoint of controller design, the valley-shaped input-output relationship is troublesome because the proportional-integral controller only assumes a monotonous input-output relationship.[23] To avoid the problem of the valley-shaped input-output relationship, we limited the stimulus frequency to the range from 0 to 10 Hz (Fig. 4B, right). A similar strategy of selecting the monotonous input-output portion was employed in a previous study.[12]

We quantified the dynamic AP response to HES using a transfer function analysis (Fig. 3B), and modeled it by a second-order low-pass filter with a pure dead time (Fig. 3C). Once the transfer function is modeled, we can construct a numerical simulator for the feedback controller design (Fig. 4A). Because the optimization of control parameters usually requires a number of trials even if the initial values are selected via classical methods such as Ziegler-Nichols' method,[23] it is impractical to determine optimal parameter values without using the simulator. The simulation results indicated that the integral gain value of 0.005 would provide rapid and stable AP regulation (Fig. 4C). Because the controller was designed via intensive simulations, AP was actually controlled at the target level with a small variance (Fig. 5B, bottom panel). Note that the current and frequency of HES were automatically adjusted and individualized via the feedback mechanism (Fig. 5A).

Bionic Strategies Using Neural Interfaces

A framework of treating cardiovascular diseases using neural interfaces is intriguing because the autonomic nervous system exerts powerful influences on the circulatory system. In previous studies, we identified the dynamic characteristics of the arterial baroreflex system and used them to design an artificial vasomotor center. The artificial vasomotor center was able to

control AP by stimulating the celiac ganglia in anesthetized rats[10,11] or the spinal cord in anesthetized cats.[12] The strength and rapidity of the neural effect on the cardiovascular system compared with that of the humoral effect[27,28] make the neural interventions desirable for the rapid and stable restoration of AP against acute disturbances such as those induced by postural changes. Gotoh et al. demonstrated that a direct neural interface to the rostral ventrolateral medulla also enabled rapid and stable restoration of AP during nitroprusside-induced hypotension in conscious rats.[29] The bionic system to control AP has also been applied in human subjects.[13]

Although the aforementioned bionic systems aimed to maintain AP against acute hypotension by increasing sympathetic nerve activity,[10-13,29] sympathoinhibition may also be required for the treatment of cardiovascular diseases accompanying sympathetic overactivity. Baroreceptor activation is one of the potential sympathoinhibitory neural modulation.[8,9] In the present study we only demonstrated a framework of short-term AP control by HES. With a development of proper implanting electrodes, however, we may be able to control AP chronically using HES. Although carotid sinus baroreceptor stimulation has a potential to treat drug-resistant hypertension,[9] it could activate peripheral chemoreflex by stimulating carotid bodies. HES may circumvent such unintentional chemoreflex activation. Another clinical implication will be the treatment of chronic heart failure. Although the vagal effect of HES was not evaluated in the present study, acupuncture stimulation may facilitate cardiac vagal activity.[30] Because chronic intermittent vagal nerve stimulation increased the survival of chronic heart failure rats,[7] chronic intermittent HES may be used as an alternative method of direct vagal nerve stimulation for the treatment of chronic heart failure.

Limitations

First, we did not identify the mechanism of HES. Because sectioning of the ipsilateral sciatic nerve abolished the AP response to HES (Fig. 6B), somatic afferent is involved in the effect of HES. In a series of studies, Longhurst et al. demonstrated that electroacupuncture activated group III and IV fibers in the median nerves and inhibited sympathetic outflow via activation of μ- and δ-opioid receptors in the rostral ventrolateral medulla.[31,32] Whether the similar mechanism underlies in the rapid-onset and short-lasting effect of HES awaits further studies.

Second, we used pentobarbital anesthesia. Although peripheral neurotransmissions of norepinephrine and acetylcholine can be assessed under the same anesthesia,[28,33] because pentobarbital can suppress many neurotransmitters in the central nervous system,[34] anesthesia may compromise the HES effect. Further studies are required to establish the utility of HES in awake conditions.

Third, we set the proportional gain of the controller at zero to avoid pulsatile changes in the HES command. However, other approaches such as that using a low-passed signal of measured AP as a controlled variable might also be effective to avoid the pulsatile variation in the HES command.

Finally, a development of implanting electrodes is the prerequisite for chronic use of HES. Intramuscular electrodes used in functional electrical stimulation might be used for HES but further refinements are clearly needed regarding the positioning of electrodes including the depth of implantation.[35,36]

In conclusion, we identified the dynamic characteristics of the AP response to acupuncture-like HES and demonstrated that a servo-controlled HES system was able to reduce AP at a prescribed target level. Although further studies are required to identify the mechanism of HES to reduce AP, acupuncture-like HES would be an additional modality to exert quantitative depressor effect on the cardiovascular system.

Appendix A

Framework of Feedback Controller

Figure 4A is a simplified block diagram of the feedback controller system utilized in the present study. The controller was based on a proportional-integral controller.[23-25] $G(f)$ represents the transfer function of the controller.

$$G(f) = -K_P + \frac{-K_I}{2\pi f j} \quad \text{(A1)}$$

where K_P and K_I denote proportional and integral gains, respectively. j represents the imaginary unit. Negative signs for the proportional and integral gains compensate for the negative input-output relationship between HES and the AP response. $H(f)$ represents a model transfer function from HES to AP determined from Protocol 3. The measured AP can be expressed as

$$AP_{Measured}(f) = H(f)HES(f) + AP_{Noise}(f) \quad \text{(A2)}$$

where $AP_{Noise}(f)$ is the AP fluctuation such as that associated with changes in animal conditions. The controller compares the measured AP with the target AP, and adjusts the HES command to minimize the difference between them according to the following equation.

$$HES(f) = G(f)[AP_{Target}(f) - AP_{Measured}(f)] \quad \text{(A3)}$$

By eliminating $HES(f)$ from the equations A2 and A3, the overall controller characteristics are described as

$$AP_{Measured}(f) = \frac{G(f)H(f)}{1 + G(f)H(f)} AP_{Target}(f) + \frac{1}{1 + G(f)H(f)} AP_{Noise}(f) \quad \text{(A4)}$$

The equation A4 indicates that if $G(f)$ is properly selected so that $G(f)H(f)$ becomes by far greater than unity, the measured AP approaches the target AP whereas the noise term is significantly attenuated over the frequency range of interest.

Appendix B

Problem with Threshold Current

We tried to adjust the intensity of HES by the stimulus current alone. When the stimulus current happened to be feedback controlled near a threshold current, however, the controller showed on-off type controller behavior around the target AP level as shown in Figure 7. At time zero, the controller was activated. The stimulus current increased to approximately 2.7 mA in the beginning and then decreased to a value below 1 mA, accompanying the AP reduction around a target level (a horizontal dashed line). However, the stimulus current and AP did not stabilize. Because the AP response was discontinuous at the threshold current (i.e., the depressor effect of HES was abruptly turned on and off), the controller could not adjust the stimulus current in a continuous manner. To avoid this kind of on-off type controller behavior, we introduced the stimulus frequency as the secondary control variable (Fig. 4B).

References

1. Bilgutay AM, Bilgutay IM, Merkel FK, Lillehei CW. Vagal tuning. A new concept in the treatment of supraventricular arrhythmias, angina pectoris, and heart failure. J Thorac Cardiovasc Surg 1968; 56: 71-82.
2. Braunwald E, Epstein SE, Glick G, Wechsler AS, Braunwald NS. Relief of angina pectoris by electrical stimulation of the carotid-sinus nerves. N Engl J Med 1967; 277: 1278-1283.
3. Schwartz SI, Griffith LS, Neistadt A, Hagfors N. Chronic carotid sinus nerve stimulation in the treatment of essential hypertension. Am J Surg 1967; 114: 5-15.
4. Vanoli E, De Ferrari GM, Stramba-Badiale M, Hull SS Jr, Foreman RD, Schwartz PJ. Vagal stimulation and prevention of sudden death in conscious dogs with a healed myocardial infarction. Circ Res 1991; 68: 1471-1481.
5. Yang JL, Chen GY, Kuo CD. Comparison of effect of 5 recumbent positions on autonomic nervous modulation in patients with coronary artery disease. Circ J 2008; 72: 902-908.
6. Baba R, Koketsu M, Nagashima M, Inasaka H, Yoshinaga M, Yokota M. Adolescent obesity adversely affects blood pressure and resting heart rate. Clr J 2007; 71: 722-726.
7. Li M, Zheng C, Sato T, Kawada T, Sugimachi M, Sunagawa K. Vagal nerve stimulation markedly improves long-term survival after chronic heart failure in rats. Circulation 2004; 109: 120-124.
8. Zucker IH, Hackley JF, Cornish KG, Hiser BA, Anderson NR, Kieval R, et al. Chronic baroreceptor activation enhances survival in dogs with pacing-induced heart failure. Hypertension 2007; 50: 904-910.
9. Mohaupt MG, Schmidli J, Luft FC. Management of uncontrollable hypertension with a carotid sinus stimulation device. Hypertension 2007; 50: 825-828.
10. Sato T, Kawada T, Shishido T, Sugimachi M, Alexander J Jr, Sunagawa K. Novel therapeutic strategy against central baroreflex failure: a bionic baroreflex system. Circulation 1999; 100: 299-304.
11. Sato T, Kawada T, Sugimachi M, Sunagawa K. Bionic technology revitalizes native baroreflex function in rats with baroreflex failure. Circulation 2002; 106: 730-734.
12. Yanagiya Y, Sato T, Kawada T, Inagaki M, Tatewaki T, Zheng C, et al. Bionic epidural stimulation restores arterial pressure regulation during orthostasis. J Appl Physiol 2004; 97: 984-990.
13. Yamasaki F, Ushida T, Yokoyama T, Ando M, Yamashita K, Sato T. Artificial baroreflex: clinical application of a bionic baroreflex system. Circulation 2006; 113: 634-639.
14. Li P, Pitsillides KF, Rendig SV, Pan HL, Longhurst JC. Reversal of reflex-induced myocardial ischemia by median nerve stimulation: a feline model of electroacupuncture. Circulation 1998; 97: 1186-1194.
15. Longhurst JC. Electroacupuncture treatment of arrhythmias in myocardial ischemia. Am J Physiol Heart Circ Physiol 2007; 292: H2032-H2034.
16. Lujan HL, Kramer VJ, DiCarlo SE. Electroacupuncture decreases the susceptibility to ventricular tachycardia in conscious rats by reducing cardiac metabolic demand. Am J Physiol Heart Circ Physiol 2007; 292: H2550-H2555.
17. Ohsawa H, Okada K, Nishijo K, Sato Y. Neural mechanism of depressor responses of arterial pressure elicited by acupuncture-like stimulation to a hindlimb in anesthetized rats. J Auton Nerv Syst 1995; 51: 27-35.
18. Uchida S, Shimura M, Ohsawa H, Suzuki A. Neural mechanism of bradycardiac responses elicited by acupuncture-like stimulation to a hind limb in anesthetized rats. J Physiol Sci 2007; 57: 377-382.

19. Michikami D, Kamiya A, Kawada T, Inagaki M, Shishido T, Yamamoto K, et al. Short-term electroacupuncture at Zusanli resets the arterial baroreflex neural arc toward lower sympathetic nerve activity. Am J Physiol Heart Circ Physiol 2006; 291: H318-H326.
20. Yamamoto H, Kawada T, Kamiya A, Kita T, Sugimachi M. Electroacupuncture changes the relationship between cardiac and renal sympathetic nerve activities in anesthetized cats. Auton Neurosci: Basic and Clinical 2008; 144: 43-49.
21. Marmarelis PZ, Marmarelis VZ. Analysis of Physiological Systems. The white noise method in system identification. New York: Plenum, 1978.
22. Snedecor GW, Cochran WG. Statistical Methods (8th ed.). University Press, Ames, Iowa, 1989.
23. Åström K, Hägglund T. PID Controllers: Theory, Design, and Tuning. (2nd ed.). Instrument Society of America, 1995.
24. Kawada T, Sunagawa G, Takaki H, Shishido T, Miyano H, Miyashita H, et al. Development of a servo-controller of heart rate using a treadmill. Jpn Circ J 1999; 63: 945-950.
25. Kawada T, Ikeda Y, Takaki H, Sugimachi M, Kawaguchi O, Shishido T, et al. Development of a servo-controller of heart rate using a cycle ergometer. Heart Vessels 1999; 14: 177-184.
26. Johansson B. Circulatory responses to stimulation of somatic afferents with special reference to depressor effects from muscle nerves. Acta Physiol Scand 1962; Suppl 198: 1-91.
27. Kawada T, Miyamoto T, Miyoshi Y, Yamaguchi S, Tanabe Y, Kamiya A, et al. Sympathetic neural regulation of heart rate is robust against high plasma catecholamines. J Physiol Sci 2006; 56: 235-245.
28. Kawada T, Yamazaki T, Akiyama T, Shishido T, Miyano H, Sato T, et al. Interstitial norepinephrine level by cardiac microdialysis correlates with ventricular contractility. Am J Physiol Heart Circ Physiol 1997; 273: H1107-H1112.
29. Gotoh TM, Tanaka K, Morita H. Controlling arterial blood pressure using a computer-brain interface. Neuroreport 2005; 16: 343-347.
30. Nishijo K, Mori H, Yosikawa K, Yazawa K. Decreased heart rate by acupuncture stimulation in humans via facilitation of cardiac vagal activity and suppression of cardiac sympathetic nerve. Neurosci Lett 1997; 227: 165-168.
31. Chao DM, Shen LL, Tjen-A-Looi S, Pitsillides KF, Li P, Longhurst JC. Naloxone reverses inhibitory effect of electroacupuncture on sympathetic cardiovascular reflex responses. Am J Physiol Heart Circ Physiol 1999; 276: H2127-H2134.
32. Li P, Tjen-A-Looi SC, Longhurst JC. Rostral ventrolateral medullary opioid receptor subtypes in the inhibitory effect of electroacupuncture on reflex autonomic response in cats. Auton Neurosci: Basic and Clinical 2001; 89, 38-47.
33. Kawada T, Yamazaki T, Akiyama T, Li M, Ariumi H, Mori H, et al. Vagal stimulation suppresses ischemia-induced myocardial interstitial norepinephrine release. Life Sci 2006; 78: 882-887.
34. Adachi YU, Yamada S, Satomoto M, Watanabe K, Higuchi H, Kazama T. et al. Pentobarbital inhibits L-DOPA-induced dopamine increases in the rat striatum: An in vivo microdialysis study. Brain Res Bull 2006; 69: 593-596.
35. Guevremont L, Norton JA, Mushahwar VK. Physiologically based controller for generating overground locomotion using functional electrical stimulation. J Neurophysiol 2007; 97: 2499-2510.
36. Hardin E, Kobetic R, Murray L, Corado-Ahmed M, Pinault G, Sakai J, Bailey SN, Ho C, Triolo RJ. Walking after incomplete spinal cord injury using an implanted FES system: A case report. J Rehabil Res Dev 2007; 44: 333-346.

Figure 1

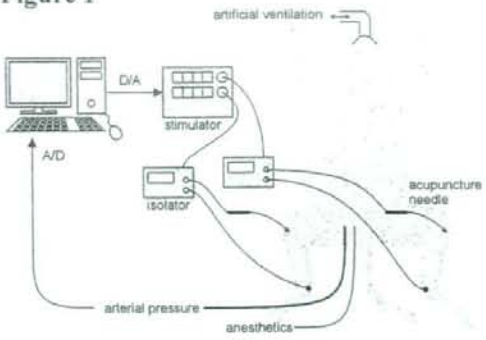

Experimental setup.

Figure 2

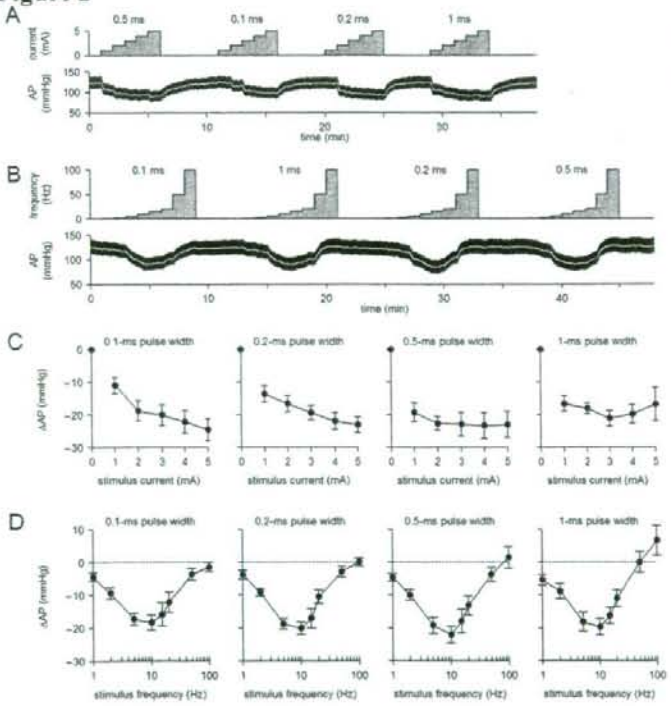

A: Typical recordings of Protocol 1 showing the effects of stimulus current and pulse width on arterial pressure (AP). **B:** Typical recordings of Protocol 2 showing the effects of stimulus frequency and pulse width on AP. The white lines in the AP traces indicate 2-s moving averaged data. **C:** Changes in AP as a function of the stimulus current. AP decreased monotonously as the stimulus current increased ($P<0.05$). **D:** Changes in AP as a function of the stimulus frequency. AP decreased more as the stimulus frequency increased from 1 to 10 Hz but the depressor effect became smaller when the stimulus frequency exceeded 10 Hz ($P<0.05$).

Figure 3

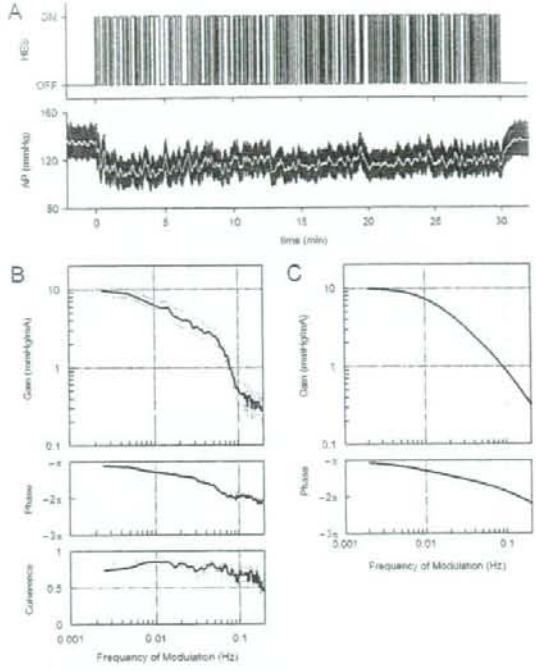

A: Typical recordings of random hind-limb electrical stimulation (HES) and arterial pressure (AP) response. **B:** Transfer function from HES to the AP response averaged from 8 cats. Thick and thin lines indicate mean and mean±SE values, respectively. **C:** A model transfer function of the second-order low-pass filter with a lag time that mimics the transfer function from HES to AP.

Figure 4

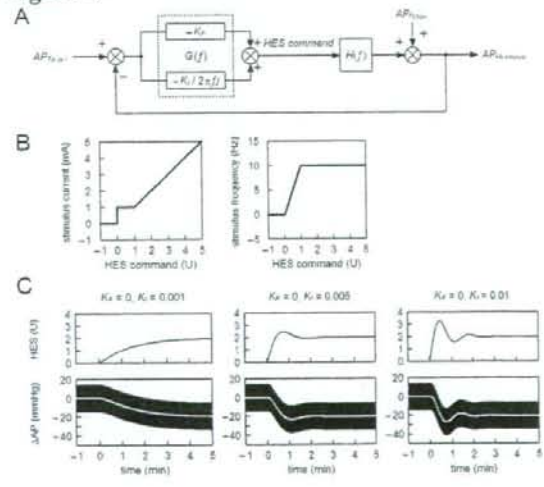

A: A simplified diagram of the feedback controller utilized in the present study. AP_{Target}: target arterial pressure (AP). AP_{Noise}: noise in AP in terms of the control theory. $AP_{Measured}$: measured AP. $G(f)$: transfer function of the controller. $H(f)$: transfer function from hind-limb electrical stimulation (HES) to the AP response. K_P: proportional gain. K_I: integral gain. f and j denote the frequency and imaginary unit, respectively (see *Appendix A* for details). **B:** Functions that convert the HES command into the stimulus current and the stimulus frequency. **C:** Simulation results showing the feedback control of AP by HES. At time zero, the target AP was set at −20 mmHg. In the simulation, a sinusoidal wave (3 Hz, 15 mmHg in amplitude) was added to mimic the pulse pressure in AP. White lines indicate the 2-s moving averaged data of the simulated AP response.

Figure 5

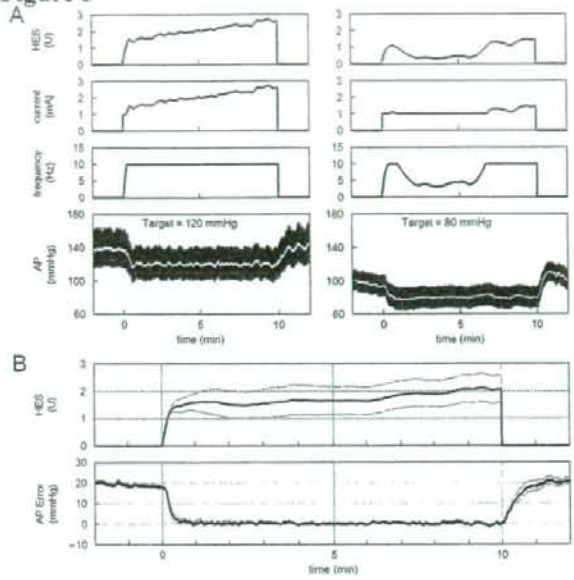

A: Results of 10-min feedback control of arterial pressure (AP) by hind-limb electrical stimulation (HES) obtained from 2 cats. In each cat, the target AP was set at 20 mmHg below the baseline AP value. The current and frequency of HES were automatically adjusted to keep the AP at the target level. **B:** HES command and the error signal between the target AP and measured AP averaged from 8 cats. The thick and thin lines indicate mean±SE values, respectively.

Figure 6

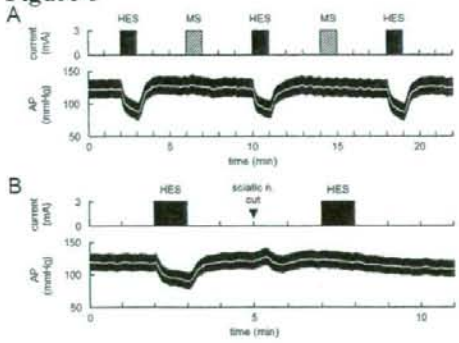

A: Effects of electrical stimulation of the triceps surae muscle (MS) in comparison to hind-limb electrical stimulation (HES). Although muscle twitching was observed, there was no change in arterial pressure (AP) during MS. **B:** Effects of sectioning the ipsilateral sciatic nerve on the HES-induced changes in AP. After the severance of the ipsilateral sciatic nerve, HES no longer produced significant hypotension.

Figure 7

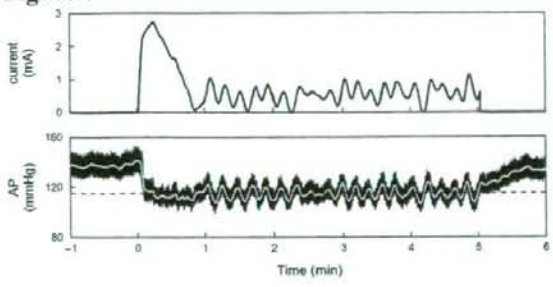

Typical recordings showing failure of controlling the intensity of the hind-limb electrical stimulation during the course of controller development. In this experimental run, only the stimulus current was controlled with a fixed stimulus frequency at 10 Hz. The controller showed on-off type controller behavior once the arterial pressure (AP) approached the target level. The horizontal dashed line indicates the target AP level.

Mini Review

Artificial Neural Interfaces for Bionic Cardiovascular Treatments

Authors: Toru Kawada, MD, PhD, and Masaru Sugimachi, MD, PhD.

Affiliations: Department of Cardiovascular Dynamics, Advanced Medical Engineering Center, National Cardiovascular Center Research Institute, Osaka 565-8565, Japan

Running head: Artificial Neural Interfaces

Correspondence:
Toru Kawada, MD, PhD.
Department of Cardiovascular Dynamics, Advanced Medical Engineering Center, National Cardiovascular Center Research Institute, Osaka 565-8565, Japan
phone: +81-6-6833-5012
Fax: +81-6-6835-5403
e-mail: torukawa@res.ncvc.go.jp

Footnote:
A part of this article is a translation from Jinkozoki (in Japanese) 35(3):352-355, 2006.